Available online at www.sciencedirect.com
SCIENCE DIRECT®
Journal of Sound and Vibration 291 (2006) 656–680
JOURNAL OF SOUND AND VIBRATION
www.elsevier.com/locate/jsvi

Simulation-based analysis of acoustic absorbent lining subject to normal plane wave incidence

C. Cai*, K.C. Hung, M.S. Khan

Institute of High Performance Computing, 1 Science Park Road #01-01, The Capricorn, Singapore Science Park II, Singapore 117528, Singapore

Received 5 October 2004; received in revised form 15 June 2005; accepted 23 June 2005
Available online 6 September 2005

Abstract

The performance of an acoustic absorbent lining can be significantly enhanced by introducing holes inside the lining. Its performance is dependent on the material properties, thickness of layers as well as the size and distribution of holes. In this paper, a simulation-based design approach that combines the acoustic finite element method (FEM) and acoustic duct method (ADM) with a multi-variable optimization technique is proposed for the design synthesis of the acoustic absorbent lining. The proposed method treats a single cell of a periodic acoustic absorbent lining in isolation. The cell may contain a set of holes. Two acoustic ducts are attached at opposing faces of the isolated cell. FEM model is built for the cell and these two acoustic ducts. The reflection and transmission characteristics of acoustic absorbent lining are calculated simultaneously using the acoustic duct theory. The zero-order optimization method is applied to optimize the various design variables, such as Young's modulus of the material, damping loss factors and the diameters of cylindrical holes, etc., to achieve the desirable acoustic performance of the absorbent lining at a single frequency of interest. The proposed method is validated against analytical solutions for a homogeneous acoustic absorbent lining. Numerical examples for the linings with different optimized results are presented to demonstrate the performance of the optimized absorbent lining.

*Corresponding author. Tel.: 65 64191205; fax: 65 64191280.
E-mail address: caic@ihpc.a-star.edu.sg (C. Cai).

0022-460X/$ - see front matter © 2005 Elsevier Ltd. All rights reserved.
doi:10.1016/j.jsv.2005.06.032

1. Introduction

A variety of acoustic absorbent lining designs has been proposed to minimize the sound reflection from the structure, such as the multi-layered gradual transmission absorbent lining, the absorbent lining using redirection of sound and mode conversion, etc. An application example of the acoustic absorbent lining is that it might be used onto the external surface of the underwater vehicles to reduce sound reflection and scattering when they are subject to acoustic wave incidence. The most compact acoustic absorbent linings are of the resonant cavity design as shown in Fig. 1. The absorbent linings are made of rubber layers containing some holes. The analysis of the acoustic absorbent lining with holes started with Oberst [1]. Later, Mayer et al. [2] studied the resonances introduced by the spherical perforations in the viscoelastic layers using a one-dimensional model. Gaunaurd [3] extended the analysis to model the deformations and oscillations occurring in the annular region conceptually constructed around one of the holes in the multi-perforated viscoelastic layer.

Most of the studies reported in the literature on sound reflection from resonant sound absorbers were done using analytical methods. The use of these methods requires not only application of special techniques but also simplifying hypotheses for the displacement field and geometry, which restricts their use only to few simple geometrical shapes. On the contrary, numerical methods have been found to be efficient and versatile in modeling the acoustic behavior of general periodic structures. Ma et al. [4,5] used the finite element method (FEM) to analyze harmonic wave propagation in viscoelastic gratings with embedded elastic fibers, and gratings with periodic distribution of cylindrical pores. Hoennion et al. [6,7] later studied the scattering of compliant tube and Alberich anechoic coatings by using FEM. Achenbach et al. [8] used the boundary element method to study the three-dimensional reflection and transmission of a plane acoustic wave by a grating composed of parallel equidistant rods. Easwaran et al. [9] presented a finite element scheme based on the Galerkin technique to analyze the reflection characteristic of the resonant absorber when insonified by a normal incidence plane wave.

In this paper, a simulation-based design method combining acoustic FEM and the acoustic duct method (ADM) with a multi-variable optimization technique is proposed for the design synthesis of the acoustic absorbent lining embedded with cylindrical holes. The paper is organized in four sections except the introduction given in current section. The mechanism of sound absorption and

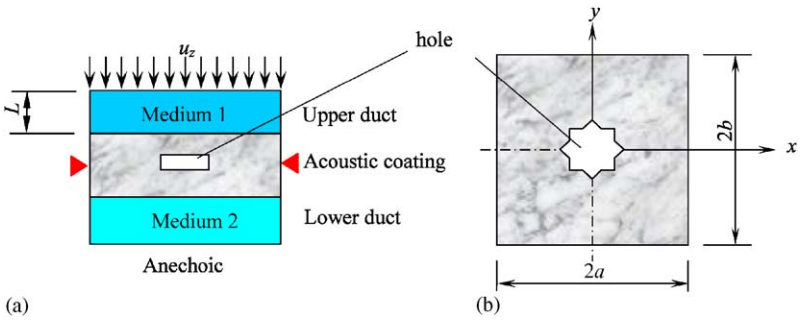

Fig. 1. A typical cell with acoustic duct method: (a) front view; (b) top view.

reflection is described in Section 2. Calculation for the sound reflection and transmission of an acoustic absorbent lining is presented in Section 3. First, an approach that combines ADM and acoustic FEM is introduced for analysis of the acoustic performance of the acoustic absorbent lining. There are two ways to implement the acoustic duct method in a FEM model. One is called the impedance transfer method in which the specific acoustic impedance at the top of the upper duct is used to compute the input specific impedance of the absorbent lining at its front surface. The other is called the direct method in which the specific impedance at any section in the upper duct is used as the input specific impedance of the absorbent lining at its front surface. A case study for a homogeneous acoustic absorbent lining reveals that the numerical results from the proposed method agreed very well with the analytical results, which provides a solid foundation for the subsequent simulation-based optimization design of the acoustic absorbent linings. Section 4 presents the zero-order optimization method for optimizing the design parameter of the absorbent lining to achieve desired acoustic characteristics at a single frequency of interest. Finally in Section 5, the performance of two optimized acoustic absorbent linings is evaluated to demonstrate the feasibility of design approach for acoustic absorbent lining with holes.

2. Sound absorption and reflection mechanism

The acoustic performance of an acoustic absorbent lining is evaluated with respect to its sound reflection and transmission coefficients,

$$R = \frac{\bar{p}^{\mathrm{re}}}{\bar{p}^{\mathrm{in}}} = \left|\frac{Z_c - Z_m}{Z_c + Z_m}\right| \quad \text{and} \quad T = \frac{\bar{p}^{\mathrm{tr}}}{\bar{p}^{\mathrm{in}}}, \tag{1}$$

where $\bar{p}^{\mathrm{re}}$ and $\bar{p}^{\mathrm{tr}}$ are the reflected and transmitted waves on the incident and transmitted sides of the absorbent lining, respectively, subject to an incident plane wave, $\bar{p}^{\mathrm{in}}$. "Bar" symbol denotes the amplitude. Z_c is the input specific impedance at the interface (front surface) between the absorbent lining and the surrounding medium on the incident side. It can be expressed as the ratio of the acoustic pressure to the particle velocity or structural vibration velocity at the top surface of absorbent lining in Eq. (2). $Z_m = \rho_m C_m$ is the characteristic specific impedance of medium. ρ_m and C_m are the density of medium and the speed of sound wave in the medium.

$$Z_c = \frac{p^{\mathrm{re}} + p^{\mathrm{in}}}{v} = \frac{p}{\mathrm{j}\omega u}, \tag{2}$$

where v and u are the structural normal velocity and displacement of the absorbent lining, respectively. p is the complex acoustic pressure consisting of both incident and reflective acoustic pressures. ω is the circular frequency $\omega = 2\pi f$, f the frequency in Hz. j is the imaginary symbol, $\mathrm{j} = \sqrt{-1}$.

From Eq. (1), it can be deduced that a perfect match between the input specific impedance of the absorbent lining and the characteristic specific impedance of medium will nullify any sound reflection from the absorbent lining.

Generally, part of incident sound wave will be reflected due to the mismatch of two impedances Z_m and Z_c while the remaining wave will transmit into the absorbent lining through its top surface and continue its journey inside the absorbent lining. For a plane harmonic acoustic incident wave

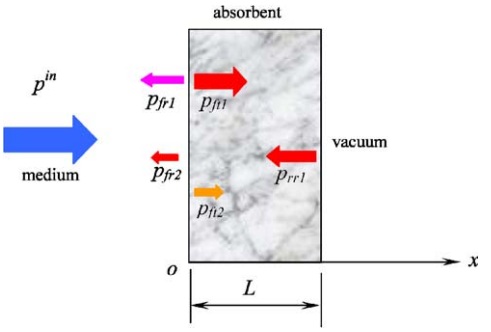

Fig. 2. An infinite structure subject to a normal plane wave incidence.

traveling in the x direction through the lossy material as shown in Fig. 2, the acoustic pressure p will decay exponentially with distance for lossy material with a linear stress–strain relation.

$$p = \bar{p}e^{j(\omega t - k^* x)} = \bar{p}e^{\alpha x}e^{j(\omega t - kx)}, \tag{3}$$

where $\bar{p}$ is the amplitude of the acoustic wave, k^* the complex wavenumber, $k^* = k + j\alpha$. The wavenumber k is $k = 2\pi/\lambda$ and λ is the wavelength. The sound attenuation coefficient α is expressed in nepers per meter.

The decay exponential, $e^{\alpha x}$, in Eq. (3) enlightens us that more acoustic energy will be dissipated if a thick acoustic absorbent lining is used because the thicker the lining, the more travelling distance the acoustic wave.

If the elastic modulus of a lossy isotropic material is expressed as a complex quantity as $E^* = E(1 + j\eta)$, in which E is the Young's modulus of the material, η the loss factor, the sound attenuation coefficient of the material can be estimated using

$$\alpha = -\frac{\pi\eta}{\lambda}. \tag{4}$$

Eq. (4) shows that the sound absorption is proportional to the loss factor of the acoustic absorbent lining and the frequency of the acoustic wave.

The mechanism of sound reflection and transmission from an acoustic absorbent lining may be illustrated in Fig. 2. An incident wave striking the vacuum-backed lossy lining will undergo the first reflection, p_{fr1}, at the top surface due to the input impedance mismatch of the medium and the absorbent lining material. The incident wave induces structure vibration of the absorbent lining. Part of the incident wave, p_{ft1}, will transmit into the absorbent lining in the form of elastic longitudinal wave. The elastic wave in the layer decays exponentially with traveling distance according to Eq. (3). The decayed traveling wave p_{ft1} will undergo a secondary reflection, p_{rr1}, upon hitting the bottom surface of the absorbent lining. The secondary reflected wave, p_{rr1}, which travels towards the sound source, will decay exponentially in the absorbent lining material until it hits the top surface. This decayed reflected wave p_{rr1} will encounter the following countereoting waves (1) the reflection traveling in x direction, p_{ft2}, and (2) transmission traveling in the medium, p_{fr2}. It is assumed that decaying waves traveling to and fro within the absorbent lining arising from p_{ft2} due to impedance mismatch at both ends of absorbent lining can be neglected because of sound dissipation effect of the absorbent lining. Taking all these into consideration, there exist

now two possible means to reduce the sound reflection from the acoustic absorbent lining. The first means is to use impedance matching concept in order to minimize the first reflection component p_{fr1} in Fig. 2. As the acoustic specific impedance Z_m of medium is a real value while the specific impedance of the acoustic absorbent lining is a complex value due to the existence of loss factor, in general, the impedance matching at the top surface of the absorbent lining is difficult to achieve hence there will always be the first sound reflection component, p_{fr1}. The second means is to increase the dissipation effects of the acoustic absorbent lining to minimize the second reflection component p_{fr2}. This can be achieved by embedding some holes in the acoustic absorbent lining to increase the dissipation effects of sound wave propagation.

The presence of voids in the absorbent lining layers allows the incoming acoustic wave to deform the layer, thus coupling some of the incoming wave to shearing motion in the layer. These shearing motions are rapidly attenuated due to the high shear damping characteristics of the structure. Although such absorbent linings have been used for many years, the mechanism involved is still not completely understood. The absorbent lining design is difficult since their performance must be tuned to the particular operating frequency of interest, and factors such as the size and geometry of the void, material properties of surrounding layers have significant impact on its performance. Therefore, the design of the sound resonant absorbent linings still requires considerable trial and error in practice.

3. Sound reflection and transmission coefficients

There exist some analytical methods to investigate the sound reflection and transmission of the acoustic absorbent lining with holes but they are restricted only to some fewer geometrical shapes. Therefore, a simulation-based method is proposed in this paper to study the acoustic performance of the absorbent lining with general geometries.

3.1. Acoustic duct method (ADM)

Following the same concept by Easwaran et al. [9] and Hoennion et al. [6,7], a conceptual region around a set of holes or a single hole is considered and studied in isolation as a cell. Two acoustic ducts are modeled above and below the acoustic absorbent lining to represent the acoustic media on incident side and transmitted side, respectively, as shown in Fig. 1. The plane wave exists in the upper duct in the frequency range below the cut-off frequency ($f = c_{m1}\sqrt{1/a^2 + 1/b^2}/4$) of the acoustic duct from the acoustic duct theory where c_{m1} is the sound speed in medium 1, and $2a$ and $2b$ are the widths of the cell in x and y directions, respectively.

If the cell does not contain any holes, the acoustic plane waves always exist in both upper and lower acoustic ducts irregardless of the length of two ducts as shown in Fig. 3a. However, if the cell contains a hole or a set of holes, the acoustic pressure distribution near the top surface of the cell may behave non-uniformly as shown in Fig. 3b. In this case, the acoustic pressure p in Eq. (2) is not uniform either. Hence, Eq. (2) cannot be applied directly to obtain the input specific impedance of the absorbent lining. To calculate this impedance, two methods are proposed with an appropriate length, L, of the upper acoustic duct.

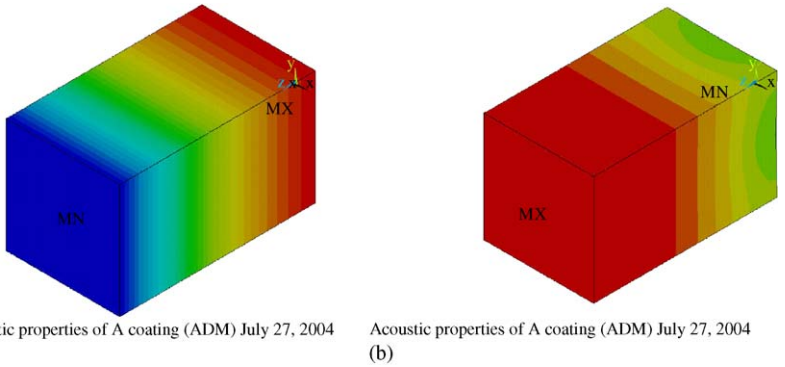

Fig. 3. Distribution of acoustic pressure near the front surface of the cell: (a) homogeneous second layer; (b) a hole in the second layer.

The advantage of ADM lies in that both acoustic reflection and transmission coefficients of absorbent lining can be evaluated simultaneously whenever the absorbent lining is with or without hole(s). In addition, the effect of medium 2 can be included on the acoustic reflection coefficients of the absorbent lining. The major disadvantage of ADM lies in that both acoustic media above and below the absorbent lining need to be modeled in FEM model. It leads to more CPU time and core memory for FEM analysis. However, if the symmetry condition of the acoustic absorbent lining is considered, CPU time and core memory may be reduced remarkably.

3.2. Boundary condition on four sides

The following boundary conditions are specified for the isolated cell in FEM model.

Referring to Fig. 1, the uniform structural displacement, u_z, is applied at the top of the upper acoustic duct to generate the plane acoustic wave impinging on the absorbent lining. The full absorbing boundary condition is prescribed on the bottom of the lower acoustic duct to represent an anechoic end. This ensures that only transmitted acoustic wave exist in the lower acoustic duct. On the other four side surfaces of FEM model, the following periodic boundary conditions are defined:

$$u_x(-a, y, z) = u_x(a, y, z) = 0, \quad u_y(x, -b, z) = u_y(x, b, z) = 0, \tag{5}$$

$$u_x(x, -b, z) = u_x(x, b, z), \quad u_y(-a, y, z) = u_y(a, y, z). \tag{6}$$

3.3. Reflection coefficients

To compute the reflection coefficient of the absorbent lining, the input specific impedance Z_c has to be obtained. Two methods are proposed with ADM to calculate the input specific impedance Z_c of the absorbent lining.

3.3.1. The impedance transfer method

The input specific impedance at the front surface of absorbent lining is calculated by use of the impedance transfer theory, if Z_d the specific acoustic impedance at the top of the upper duct is known:

$$Z_c = \rho_{m1} c_{m1} \frac{\cos(kL) Z_d - \mathrm{j}\rho_{m1} c_{m1} \sin(kL)}{\rho_{m1} c_{m1} \cos(kL) - \mathrm{j} \sin(kL) Z_d}, \tag{7}$$

where ρ_{m1} is the density of medium 1, L the length of the acoustic duct shown in Fig. 1.

Because plane acoustic waves exists near the upper region in the upper acoustic duct, Z_d can be calculated as Eq. (8).

$$Z_d = \frac{p}{\mathrm{j}\omega u_z} = \frac{p_r + \mathrm{j}p_i}{\mathrm{j}\omega u_z}, \tag{8}$$

where p_r and p_i are the real and imaginary components of the acoustic pressure at the top of the upper duct, respectively. u_z is the specified displacement in z-axis at the top of the upper acoustic duct.

Substitution of Eq. (8) into Eq. (7) leads to

$$Z_c = \rho_{m1} c_{m1} \frac{[p_r \cos(kL) + \rho_{m1} c_{m1} \omega u_z \sin(kL)] + \mathrm{j}p_i \cos(kL)}{p_i \sin(kL) + \mathrm{j}[\rho_{m1} c_{m1} \omega u_z \cos(kL) - p_r \sin(kL)]}. \tag{9}$$

From the input specific impedance at the front surface of absorbent lining, Z_c, the reflection coefficient can be calculated using Eq. (1).

3.3.2. The direct method

From the derivation of Eq. (1) using the acoustic duct method, it is found that Z_c may refer to the specific impedance at any section of the upper duct where the plane wave exists. In other word, Z_c in Eq. (1) can be replaced directly with Z_d in Eq. (8) when calculating the reflection coefficient of the acoustic absorbent lining.

Both methods, the impedance transfer method and the direct method, give the same reflection coefficient results.

3.4. Transmission coefficients

The standing acoustic pressure, $\bar{p}$, in the upper acoustic duct consists of two pressures corresponding to opposing progressive waves, i.e. incident and reflected acoustic waves. Once the reflection coefficient, R, is obtained, the incident acoustic pressure in the upper duct can be evaluated as

$$\bar{p}^{\mathrm{in}} = \frac{\bar{p}}{1 + R}. \tag{10}$$

The acoustic pressure in the lower acoustic duct only consists of the pressure corresponding to the transmitted pressure, $\bar{p}^{\mathrm{tr}}$. It is because the lower end of the bottom acoustic duct is

non-reflective. Therefore, the transmitted coefficient can be obtained from Eq. (1) as

$$T = \frac{\bar{p}^{\mathrm{tr}}}{\bar{p}}(1+R). \tag{11}$$

3.5. Validation

To validate the proposed simulation-based method for analysis of acoustic performance of acoustic absorbent lining, the sound reflection and transmission from a three-layer absorbent lining structure is investigated in case 1. The third layer is the base structure where the acoustic absorbent lining is pasted. The first two layers are actually the acoustic absorbent lining. In case 1, the selected absorbent lining structure does not contain any holes, i.e., each layer is homogeneous, because the analytical results [10–12] of reflection and transmission coefficients can be found for comparison purpose. The geometrical dimension and the properties of the upper, lower acoustic media and the acoustic absorbent lining are listed in Tables 1 and 2.

The FEM model for the acoustic absorbent lining structure is created using FEM code ANSYS which includes the fluid models for upper and lower acoustic ducts as well as structural models for three layers as shown in Fig. 4. The mesh size follows that a $\lambda/12$ criterion is applied on the shear waves and a $\lambda/4$ criterion on the flexural wavelength [9]. The element types used in ANSYS FEM model are listed in Table 3.

The comparison between analytical and ADM results is shown in Fig. 5. Excellent agreements are observed between two results, thus, providing a strong validation for the simulation-based method proposed.

To further validate the model, two more examples are cited to validate our results against those in Refs. [9,7]. In the first example, an Alberich lining made of silicone immersed in fluid is made up

Table 1
Geometrical and material properties of the acoustic absorbent lining

	1st layer	2nd layer	3rd layer
Young's modulus (N/m^2)	1000	4×10^8	2.1×10^{11}
Density (kg/m^3)	29	1800	7800
Poisson's ratio	0.495	0.495	0.3
Loss factor	1.6582	1.991	0.001
Thickness (m)	0.0088	0.001	0.025

Table 2
Geometrical and material properties of the acoustic ducts

	Upper duct	Lower duct
Density (kg/m^3)	1.12	1.12
Sound speed (m/s)	340	340
Length of the duct (m)	0.05	0.05

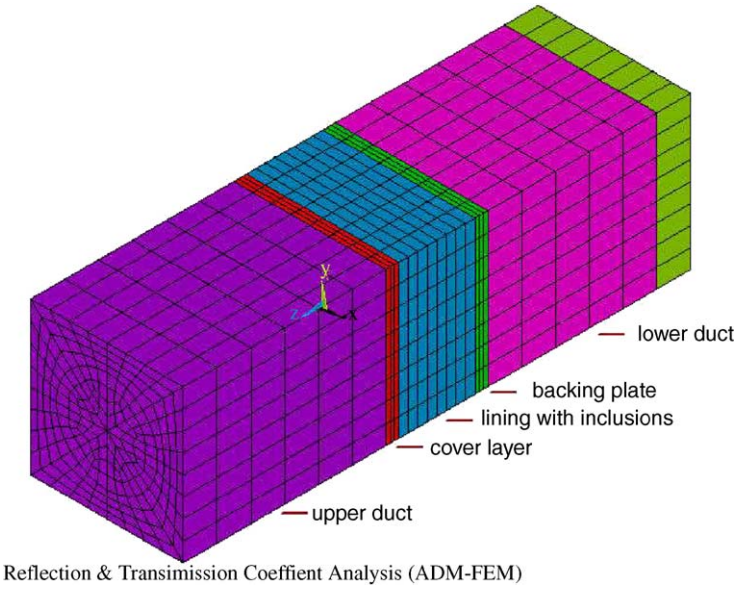

Fig. 4. FEM model using simulation-based method in case 1.

Table 3
Element types used in ANSYS FEM model

S/N	Element type	Applicable to
1	ET,1,fluid30, ,1	Fluid not-touching structures in upper duct
2	ET,2,fluid30	Fluid touching structures in upper duct
3	ET,3,solid45	Cover layer
4	ET,4,solid45	Lining with inclusions
5	ET,6,solid45	Backing plate
6	ET,7,fluid30, ,1	Fluid not-touching structures in lower upper duct
7	ET,8,fluid30	Fluid touching structures in lower duct

of a layer of silicone containing air inclusions. The density and sound speed of the fluid are assumed to be 1000 kg/m^3 and 1489 kg/m. The lining is 4 cm thick with a grating spacing 5 cm, and cylindrical inclusions of 2 cm height and 1.5 cm diameter. The properties of the panel material are $E = 1.8 \times 10^6$ Pa, $\rho = 1000$ kg/m^3, $\upsilon = 0.49976$ the loss factor is 0.15. The geometry of the Alberich lining refers to Fig. 6.

It can be seen from Fig. 7 that there is a good agreement of the results obtained using the present method and those obtained experimentally.

In the second example, the lining immersed in fluid is made up of a layer of viscoelastic material containing air inclusions. The lining is 2 cm thick with a grating spacing 3 cm, and cylindrical inclusions of 1.5 cm height and 2 cm diameter, referring to Fig. 6. The properties of the lining material are $E = 1.4 \times 10^8$ Pa, $\rho = 1100$ kg/m^3, $\upsilon = 0.49$ the loss factor is 0.23. (It is noted that

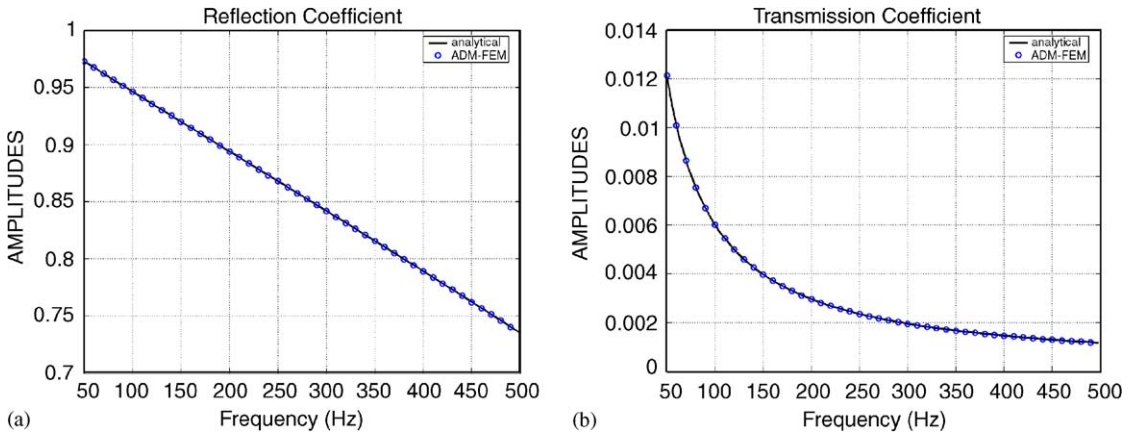

Fig. 5. Comparison of reflection and transmission coefficients: (a) reflection coefficients; (b) transmission coefficients.

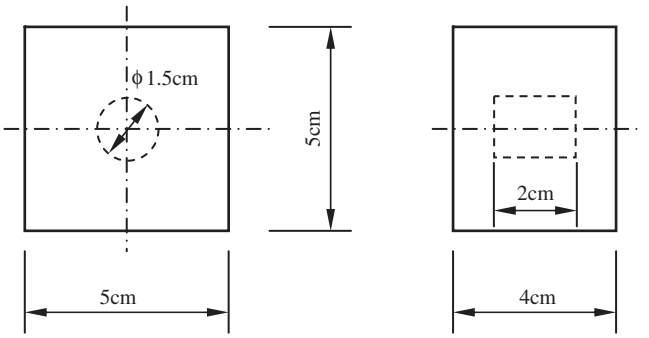

Fig. 6. Schematic of a cell of silicone Alberich lining.

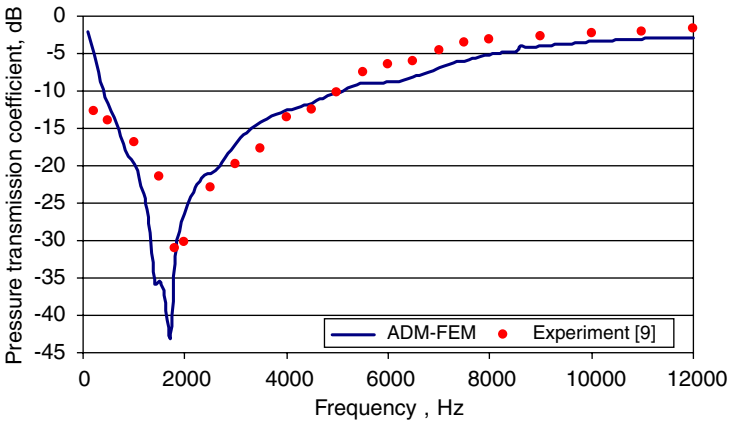

Fig. 7. Pressure transmission coefficient of silicone Alberich lining (1st example).

both Refs. [7,9] used $E = 1.4 \times 10^9$ Pa.) t can be seen from Fig. 8 that there is an excellent agreement of the results obtained using the present method and those obtained in Refs. [7,9].

Subsequently, a three-layer acoustic absorbent lining with periodic vacuum-empty holes in the second layer is considered to investigate the acoustic performance of the 'absorbent lining using the proposed method and optimization. All the geometrical dimensions and material properties follow Tables 1 and 2 except for the distributed "empty" holes in the second layer. The default radius of a hole is 0.004 m. The spacing, s, between two holes is 0.03 m.

A cell which contains a cylindrical vacuum-empty hole as shown in Fig. 9a is extracted and analyzed using the proposed simulation-based method. Fig. 10 shows the acoustic reflection and transmission coefficients of the acoustic absorbent linings with and without holes. The solid curve represents the results for the absorbent lining without any holes in the second layer. The solid curve with circles shows the results when holes are embedded in layer 2. The figure indicates that the holes in the acoustic absorbent lining can modify its acoustic performance spectrum. The acoustic reflection coefficient of the absorbent lining with holes decreases while the acoustic

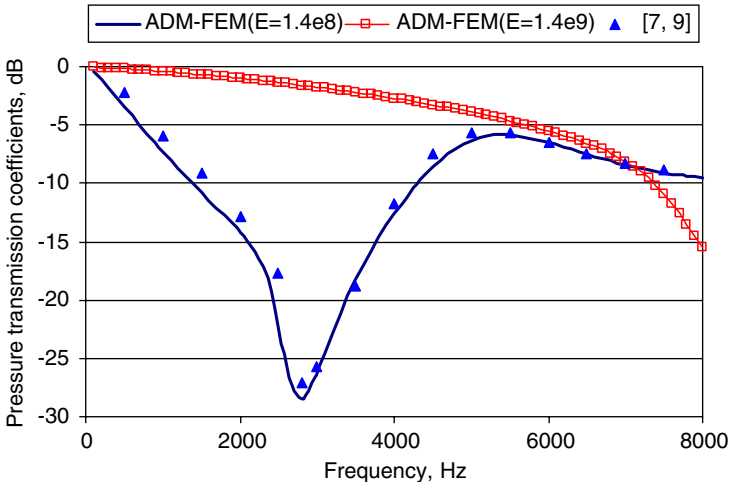

Fig. 8. Pressure transmission coefficient of Alberich lining (the 2nd example).

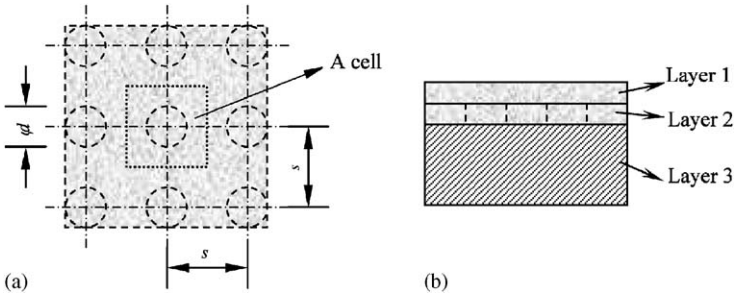

Fig. 9. Schematic of acoustic absorbent lining with holes: (a) top view; (b) front view.

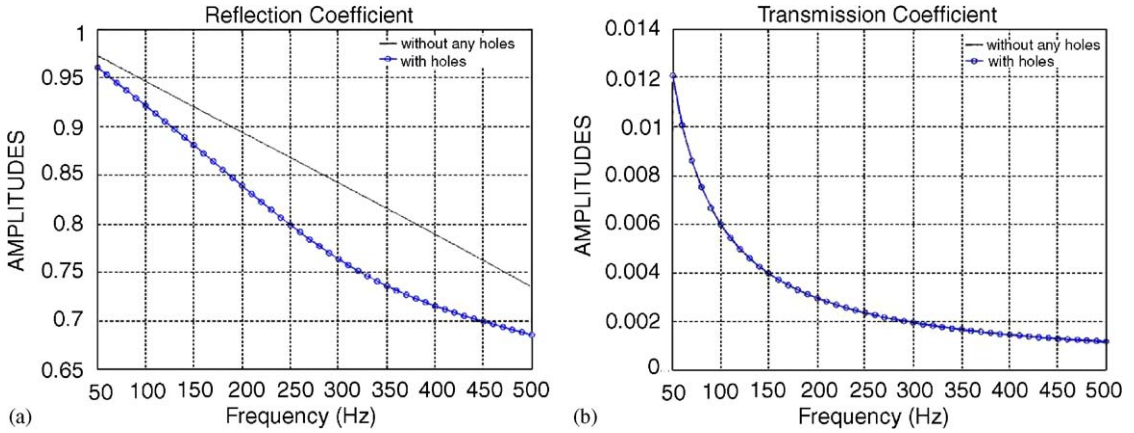

Fig. 10. Reflection and transmission coefficients of the absorbent linings: (a) reflection coefficients; (b) transmission coefficients.

transmission coefficients of the absorbent lining with holes and without holes are almost identical. To make use of the holes effectively and to make the absorbent lining work at the frequency of interest, the geometrical and material properties of the absorbent lining need to be optimized.

4. Optimization of the acoustic absorbent lining

To tailor the properties of the acoustic absorbent lining to meet the acoustic reflection requirement at the frequency of interest, the design optimization for the structural and material parameters is needed. For the given absorbent lining geometry as shown in Fig. 9, the following nine design variables (DVs) are defined in the optimization process.

In this paper, the objective function is to minimize the acoustic reflections of the absorbent lining at a single target frequency as,

$$f = \min[R(\mathbf{x})] \quad \text{at single frequency of interest,} \tag{12}$$

where $\mathbf{x}$ is the vector containing all or part of DVs in Table 4. R stands for the reflection coefficient.

4.1. Zero-order optimization method [13]

Zero-order method is employed to optimize the design variables for the desirable acoustics performance. First, a new objective function is constructed approximately by means of least-squares fitting. Next, the constrained minimization problem to the approximated objective function is converted to an unconstrained problem using penalty functions. Finally, the minimization is performed at every iteration on the penalized and approximated objective function until convergence is achieved or termination target is reached.

Table 4
Selection of design variables

	1st layer	2nd layer
Thickness	√	√
Young's modulus	√	√
Density	√	√
Loss factor	√	√
Hole diameter		√

The new objective function $\hat{f}$ is constructed as

$$\hat{f}(\mathbf{x}) = f(\mathbf{x}) + error \text{ at target frequency}, \tag{13}$$

where

$$\hat{f}(\mathbf{x}) = a_0 + \sum_{i=1}^{n} a_i x_i + \sum_{i}^{n} \sum_{j}^{n} b_{ij} x_i x_j. \tag{14}$$

Symbol ˆ notation represents an approximation. n is the total number of design variables. x_i is one of design variables. f is the original objective function in Eq. (12).

The coefficients, a_i and b_{ij}, in Eq. (14) are determined with a weighted least-squares technique. For example, the weighted least-squares error norm for the objective function has the form

$$E^2 = \sum_{i=1}^{n_d} \phi^{(i)} (f^{(i)} - \hat{f}^{(i)})^2, \tag{15}$$

where $\phi^{(i)}$ is a weight associated with design set *i.* n_d is current number of design sets. One design set means a set of design variables during optimization. Each optimization loop will generate a new set of design variables, therefore, the new approximated objection function will be updated accordingly.

Eq. (14) shows the relationship between the approximated objective function and the design variables. The coefficients in the equation are determined by minimizing E^2 with respect to the coefficients.

With approximated objective function obtainable after determination of all coefficients in Eq. (14), the constrained minimization problem becomes:

$$\min[\hat{f} = \hat{f}(x)], \tag{16}$$

subject to

$$\underline{x}_i \leqslant x_i \leqslant \bar{x}_i \quad (i = 1, 2, 3, \ldots, n), \tag{17}$$

where $\underline{x}_i$ and $\bar{x}_i$ are the lower and upper limits of respective design variables.

Next, the constrained optimization problems as Eqs. (16) and (17) are converted to unconstrained ones by means of penalty functions [13]. Finally, a sequential unconstrained minimization technique is used to search for a minimum unconstrained approximated objective function.

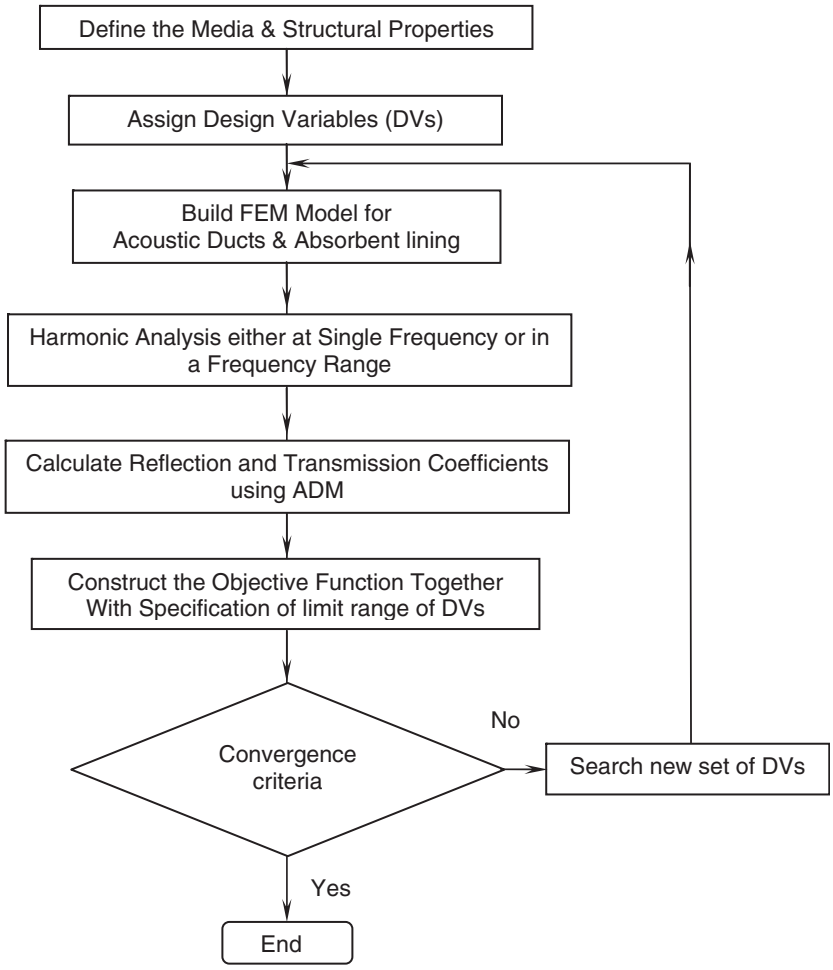

Fig. 11. Optimization flow chart implemented in ANSYS.

The flow chart of optimization is shown in Fig. 11 which has been implemented with ANSYS. Two sub-case studies are considered using the simulation-based design and zero-order optimization methods. First, only two design variables, the hole's diameter and the thickness of the second layer, are selected during optimization from the nine DVs listed in Table 4. Second, all nine design variables are selected.

4.2. Optimization with two design variables (case 2)

Two design variables refer to the hole's diameter and the thickness of the second layer. The design variable vector is expressed as

$$\mathbf{x} = \begin{Bmatrix} \phi d \\ \text{th\_}l_2 \end{Bmatrix}, \tag{18}$$

subject to the following constraints with upper and lower limits:

$$0.002 \leqslant \phi d \leqslant 0.020 \tag{19}$$

and

$$0.001 \leqslant \text{th\_}l_2 \leqslant 0.050. \tag{20}$$

The target frequency is 250 Hz.

After optimization, two design variables become $\phi d = 0.017\,\text{m}$ and $\text{th\_}l_2 = 0.023\,\text{m}$ as the reflection coefficient decreases from 0.80 to 0.62 at target frequency 250 Hz. Fig. 12 shows the reflection and transmission coefficients of the acoustic absorbent lining with the two optimized design variables together with other geometrical and material properties listed in Tables 1 and 2. The reflection coefficients of the absorbent lining decrease in the frequency range below 450 Hz. The minimum reflection coefficient point does not occur at target frequency 250 Hz but around 150 Hz. This is due to the fact that selected two design variables are not enough to define the optimized acoustic absorbent lining for minimum reflection coefficient at this particular frequency. The transmission coefficient meantime decreases in the whole frequency range as well. To check if the minimum reflection coefficient occurs at target frequency 250 Hz, all nine design variables are investigated next as case 3.

4.3. Optimization with nine design variables (case 3)

All nine design variables in Table 4 are taken into account for the minimization of sound reflection coefficient at target frequency 250 Hz. Table 5 shows the initial values, lower and upper bounds, and final optimized values of all design variables.

The reflection and transmission coefficients of the absorbent lining with nine optimized design variables are shown in Fig. 13. The reflection coefficient, 0.29, occurs around target frequency 250 Hz but the minimum reflection coefficient appears around 270 Hz. It implies that the as many

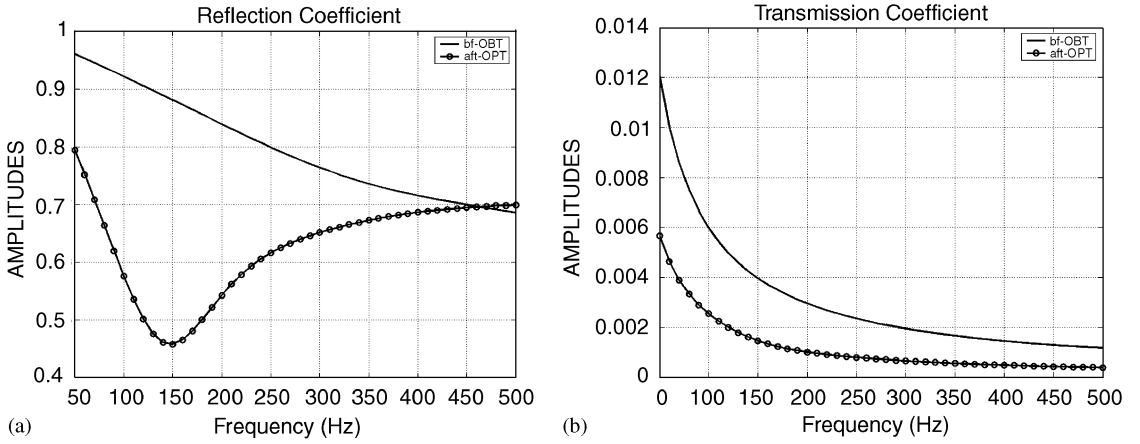

Fig. 12. Reflection and transmission coefficients with two optimized DVs: (a) reflection coefficients; (b) transmission coefficients.

Table 5
Geometrical and material properties in optimization of nine DVs

DVs	Initial value	Lower and upper bounds	Final optimized values (250 Hz)
YoungModulus-l_1 (N/m^2)	1000	500–2000	559.77
Density_l_1 (kg/m^3)	29	25–400	167.99
Thickness_l_1 (m)	0.0088	0.001–0.01	0.9717×10^{-2}
LossFactor_l_1	1.6582	0.006–2	0.3379
Diameter (m)	0.008	0.002–0.02	0.2658×10^{-2}
YoungModulus_l_2 (N/m^2)	4×10^8	4×10^8–5×10^{10}	7.5652×10^8
Density_l_2 (kg/m^3)	1800	1200–2000	1581.9
Thickness_l_2 (m)	0.001	0.001–0.050	0.4895×10^{-1}
LossFactor_l_2	1.991	0.006–2	1.9873
	Reflection coefficient		0.2949

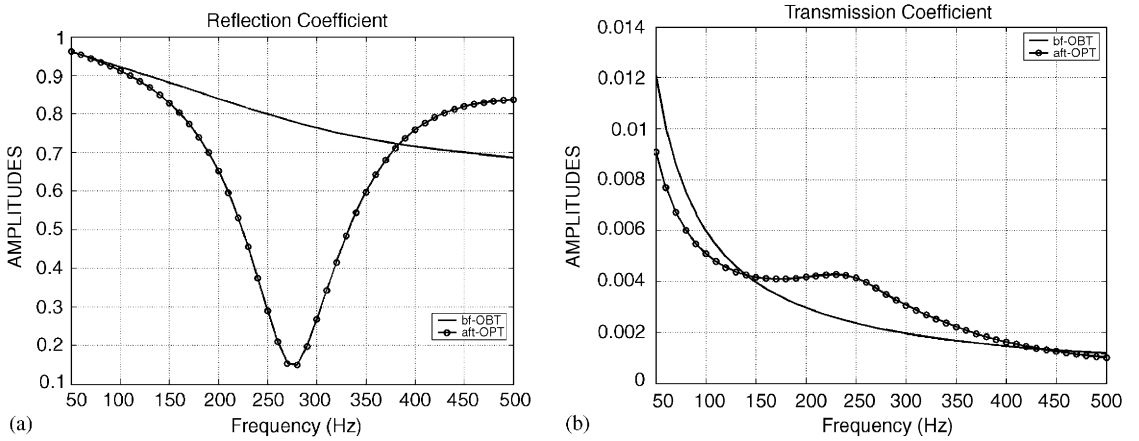

Fig. 13. Reflection and transmission coefficients with nine optimized DVs: (a) reflection coefficients; (b) transmission coefficients.

design variables should be included in optimization so that the acoustic-induced response properties of the final acoustic absorbent lining may be tuned to achieve the less reflection coefficient around the target frequency.

It is needed to point out that in practice, the design variables should be selected with regard to the reality of the situation. The dimensions and variables on which one has no control should be fixed or not be chosen as the design variables.

5. Results and discussions

The working mechanism of the acoustic absorbent lining with voids have been discussed in previous literatures. First, Gaunaurd [3] assumed that the acoustic performance is associated with

a resonance of the cylindrical hole in the second layer. The resonant frequency and the peak anechoic response occur at the same frequency. Later, Lane [14] found a contrary phenomenon, the acoustic performance of the absorbent lining is associated with the dynamic behaviour of the first layer rather than the second layer. This agrees with Oberst's proposal that a 'diaphragm' resonance of the first layer over the cylindrical holes is a possible anechoic mechanism [1]. Lane [14] quoted other researcher's suggestion as the frequency of peak anechoic performance of the absorbent lining can correspond to anti-resonance. Gaunaurd [15] in his comments on Lane's paper [14] pointed out there are actually two types of resonance mechanisms, one is due to the radial motion of the hole wall and the other to the flexural or drum-like up-and-down motion of the first layer. One will be dominant over the other depending on the stiffness of the second layer relative to that of the first and/or the third layer. If the first and third layers are relative stiff compared to the second layer, the radial motion of the hole wall will be the only one present. If the second layer is as stiff as the third layer, the only remaining motion will be the flexural, drum-like motion of the first layer.

To further understand the possible anechoic mechanism of the acoustic absorbent linings with holes, the deformations of the first two layers are investigated at selected frequencies of interest. The vibration energy dissipation in the first two layers is evaluated and compared. Finally, the uncoupled modal analysis of three structural layers in acoustic absorbent lining is carried out as well.

5.1. *Deformations of the first two layers*

The dotted lines in all the figures below indicate the layer location without deformation while the solid lines represent the deformed location of the layer.

Fig. 14 shows the deformations of the first two layers when there is no hole in the second layer of the absorbent lining. Both layers undergo the deformations in the "thickness" mode only. It means that both layers deform either compressively or extensively. The shear deformation mode does not occur.

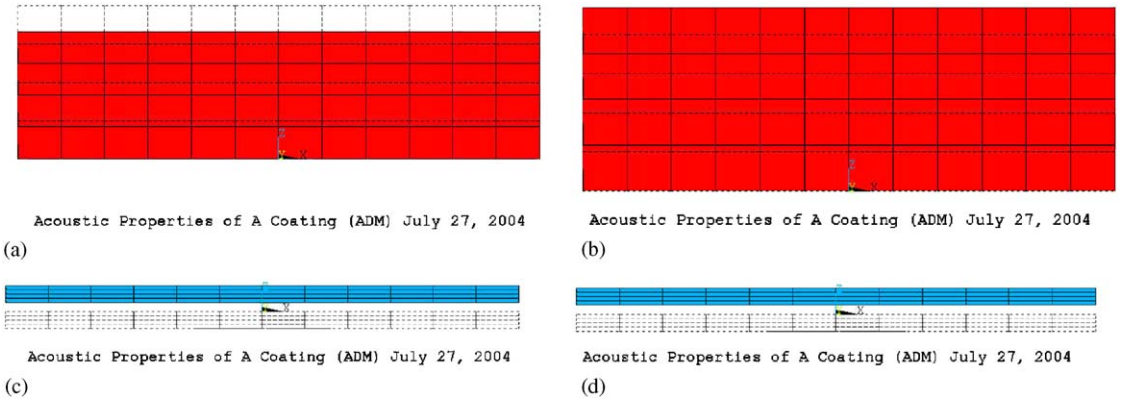

Fig. 14. Deformations of the first two layers at 250 Hz (no hole): (a) real part of the 1st layer; (b) imag part of the 1st layer; (c) real part of the 2nd layer; (d) Imag part of the 2nd layer.

5.1.1. Results for case 2

Fig. 15 shows the deformations of the first two layers when a cylindrical hole exists in the second layer with a diameter $\phi d = 0.017$ m and thickness th_$l_2 = 0.023$ m (with optimized results in case 2). Fig. 15a, c show the real components of the deformation of the first and second layers while Fig. 15b, d indicate the imaginary components of the deformation of the first and second layer at 250 Hz. It is seen that the first layer undergoes not only extensional/compressive deformation but also the shear deformation due to the bulge in the central region of the first layer. It is observed that the second layer undergoes the deformation in thickness direction only. It supports the observation on the flexural motion of the first layer in Refs. [14,15] if the stiffness of the first layer is relatively smaller compared to that of the second layer. However, it is found that other parameters beside the stiffness of layers also affect the resonance mechanisms. For case 3, nine design variables are used in the optimization.

Because the reflection coefficient around frequency 150 Hz is smaller than that at target frequency 250 Hz as shown in Fig. 12a, the deformations of the first two layers of the absorbent lining at 150 Hz are shown in Fig. 16.

The deformations of the first layer behave closer to a pure flexural motion in Fig. 16a compared to that in Fig. 15a. The second layer undergoes the motion in thickness mode at frequency 250 Hz.

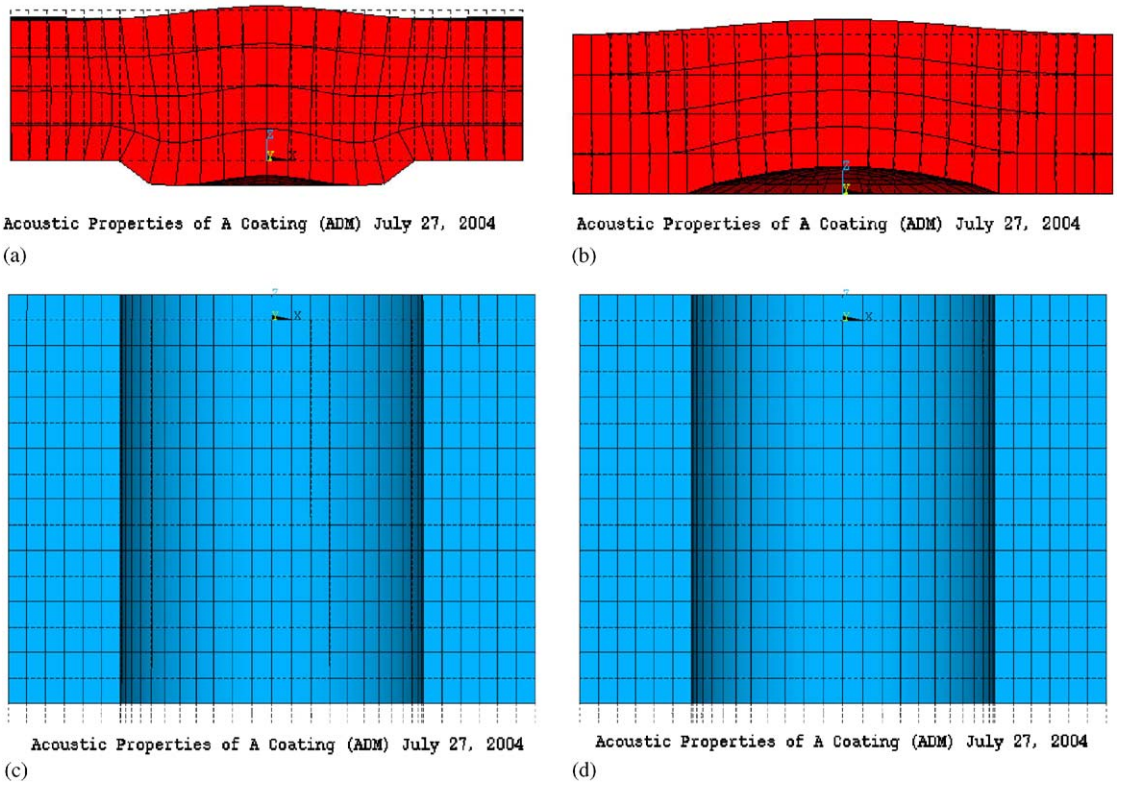

Fig. 15. Deformations of the first two layers in case 2 at 250 Hz: (a) real part of the 1st layer; (b) imag part of the 1st layer; (c) real part the of 2nd layer; (d) Imag part of the 2nd layer.

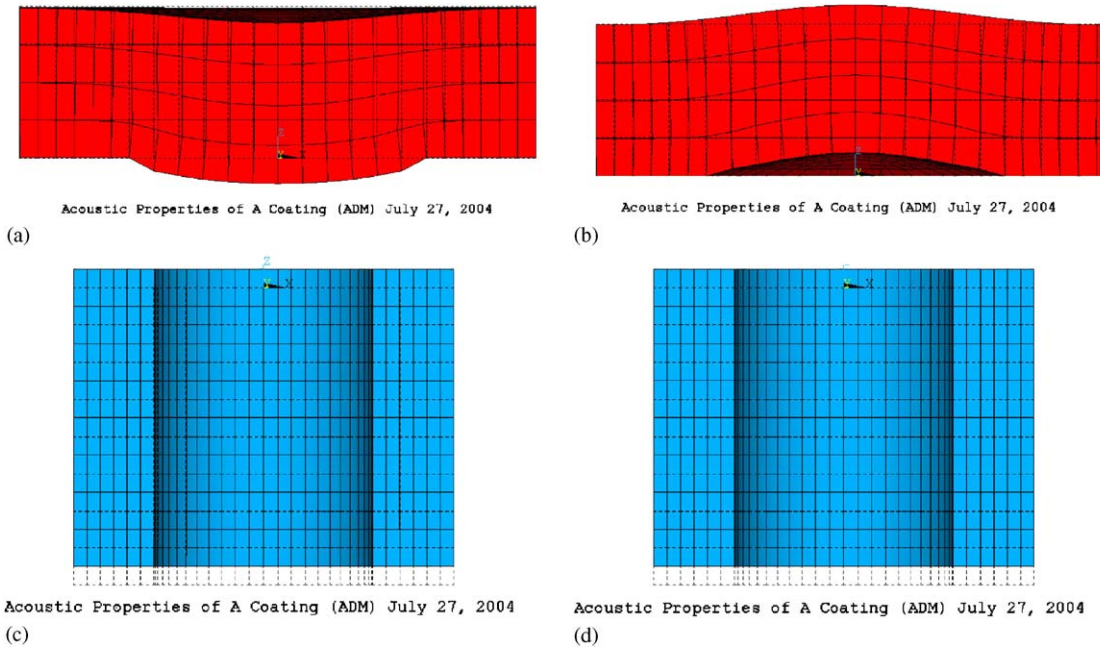

Fig. 16. Deformations of the first two layers in case 2 at 150 Hz: (a) real part of the 1st layer; (b) imag part of the 1st layer; (c) real part the of the 2nd layer; (d) Imag part of the 2nd layer.

5.1.2. *Results for case 3*

Fig. 17 shows the deformations of the first two layers of the absorbent lining (with optimized results in case 3) at target frequency 250 Hz. Fig. 17c1–c3 show the real deformation components of the upper and lower parts of the second layer as well as the real deformations viewed in top, respectively. Fig. 17d1–d3 show the imaginary components of deformations accordingly.

The first layer mainly undergoes the deformation in the thickness direction except the region above the cylindrical hole. The radial deformation above and near the central cylindrical hole in the second layer is observed although the radial deformation is smaller compared to that in thickness direction. Comparatively, the second layer has obviously not only the deformation in thickness direction but also the radial deformation from Fig. 17d1–d3. Top view of the imaginary part of deformations of layer two in Fig. 17d3 indicates that the number of circumferential waves is 4 around the cylindrical hole.

From the comparison of design variables after and before optimization listed in Table 6, the values of two design variables, the thickness of the second layer and the diameter of the hole in the second layer, become larger after optimization in case 2. However, the thickness of the second layer is increased further while the diameter of the hole in the second layer decreases after optimization in case 3. It is noted that the Young's modulus of the first layer becomes smaller and that of the second layer becomes larger. Because the Young's modulus of a material is proportional to the stiffness of the material, the simulation results of this paper reveal that the resonance mechanism of the acoustic absorbent lining depends on not only the stiffness ratio among each layer but also other geometrical and material properties.

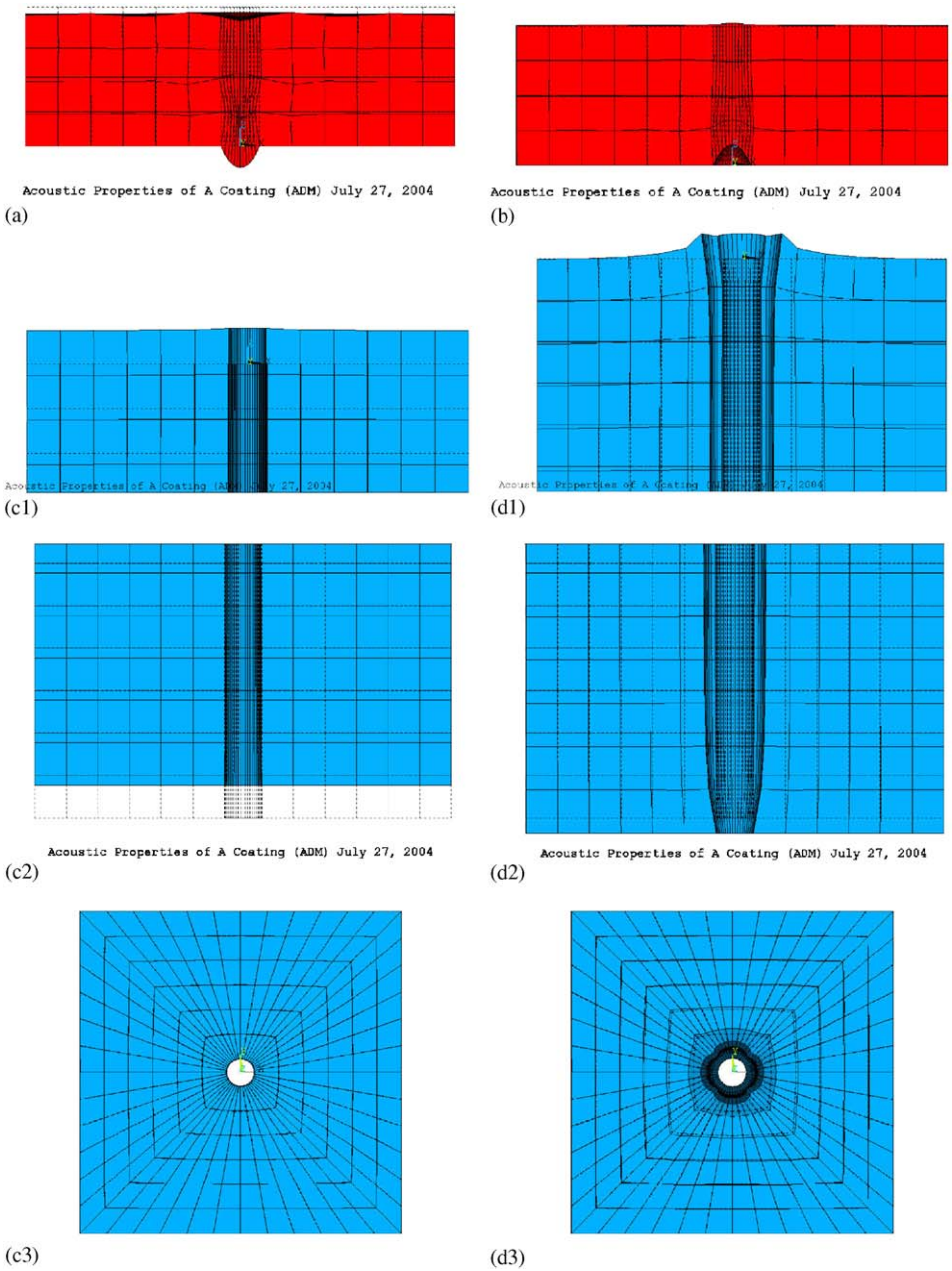

Fig. 17. Deformation of the two absorbent lining layers in case 3 at 250 Hz: (a) real part of 1st layer; (b) imag part of 1st layer; (c1) real part of upper part of 2nd layer; (c2) real part of lower part of 2nd layer; (c3) real part of 2nd layer in top view; (d1) imag part of upper part of 2nd layer; (d2) imag part of lower part of 2nd layer; (d3) imag part of 2nd layer in top view.

5.2. Potential energy dissipated in respective layers

Potential energies stored in the layers of the acoustic absorbent lining can be evaluated as

$$PE = \frac{1}{2}\oint_{V_i} \boldsymbol{\sigma}^{\mathrm{T}}\boldsymbol{\varepsilon}\,\mathrm{d}V, \tag{21}$$

where $\boldsymbol{\sigma}$ and $\boldsymbol{\varepsilon}$ are the stress and elastic strain vectors, respectively. V_i is the volume the ith layer occupies.

The potential energies corresponding to the real and imaginary parts of complex solution are extracted from each layers in FEM model via reading the real part or imaginary part of solutions, respectively. In two sub-cases of optimization, the results of potential energies for the three layers are listed at target frequency 250 Hz in Table 7.

As the product of the potential energy (the sum of the real and imaginary parts of potential energy) in a layer and the loss factor of the layer is proportional to the energy dissipated in the layer as Eq. (22), it is also listed in the table.

$$\mathrm{PELF} = \mathrm{PE}_q \times \eta_q \propto (\text{Dissipated energy})_q, \tag{22}$$

where $\mathrm{PE}_q = (\mathrm{PE}_r + \mathrm{PE}_i)_q$. PE_r and PE_i are the real and imaginary parts of the potential energy stored in a layer, respectively. Subscript q denotes the qth layer. PELF represents the product of the potential energy PE and the loss factor in the qth layer.

Table 6
Comparison of DVs after and before optimization

		Initial	Case 2	Case 3
1st layer	Young's modulus (N/m^2)	1000		559.77
	Density (kg/m^3)	29		167.99
	Loss factor	1.6582		0.3379
	Thickness (m)	0.0088		0.0097
2nd layer	Young's modulus (N/m^2)	4×10^8		7.562×10^8
	Density (kg/m^3)	1800		1581.9
	Loss factor	1.991		1.8973
	Thickness (m)	0.001	0.023	0.048
Hole	Diameter (m)	0.008	0.017	0.003

Table 7
Potential energies in the layers at target frequency 250 Hz (Joule)

Layer no	Case 2			Case 3		
	PE_r	PE_i	PELF	PE_r	PE_i	PELF
Layer 1	3.776	2.942	11.140	6.621	1.202	2.643
Layer 2	0.123×10^{-3}	0.474×10^{-5}	2.543×10^{-4}	0.193×10^{-3}	0.999×10^{-3}	2.262×10^{-3}
Layer 3	0.107×10^{-6}	0.412×10^{-6}	0.519×10^{-9}	0.407×10^{-6}	0.168×10^{-8}	0.409×10^{-9}

Table 8
Relative comparison of energy dissipated in first two layers

Layer no.	250 Hz	
	Case 2	Case 3
Layer 1	1	1
Layer 2	0.228×10^{-4}	8.559×10^{-4}
Layer 3	0.465×10^{-10}	1.547×10^{-10}

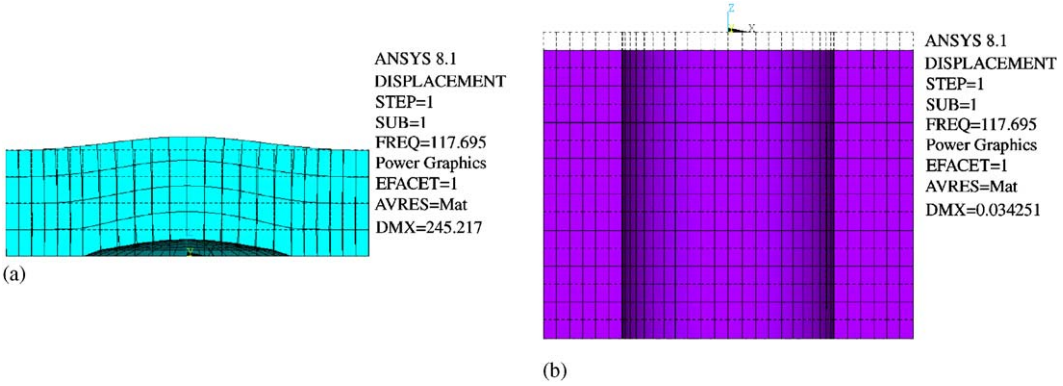

Fig. 18. Modal shape at 117.7 Hz in case 2: (a) modal shape of 1st layer; (b) modal shape of 2nd layer.

It is seen from Table 8 that most vibration energy of the absorbent lining is dissipated in the first layer in both sub-cases because more deformation exists in the first layer as shown in Figs. 15 and 17. After optimization, the thickness of the first layer in two sub-cases is almost same, 0.0088 m (case 2) and 0.0097 m (case 3). It means that the volumes of the first layer in two sub-cases are almost same. On the other hand, the thickness of the second layer in case 3 is nearly doubled compared to that in case 2, from 0.023 to 0.048 m. It means that the volume of the second layer in case 3 is around two times more than that in case 2. However, the capability of energy dissipation in the second layer is increased around 37 times in case 3 than in case 2 at target frequency 250 Hz. It shows that the more vibration energy can be dissipated in the second layer for the second resonance mechanism, that the radial motion of the second layer is dominant, than for the first resonance mechanism, that the drum-like up-and-down motion of the first layer is dominant. Based on the reflection coefficients, the second resonance mechanism in case 3 seems more effective to reduce sound reflection than the first resonance mechanism.

5.3. Modal analysis of three structural layers

It is carried out the uncoupled modal analysis of the three layers of absorbent lining with the existence of a hole in the second layer. The modal shape at each mode is checked and compared with the deformed shape of the layers from Figs. 15 to 17 at the target frequency 250 Hz.

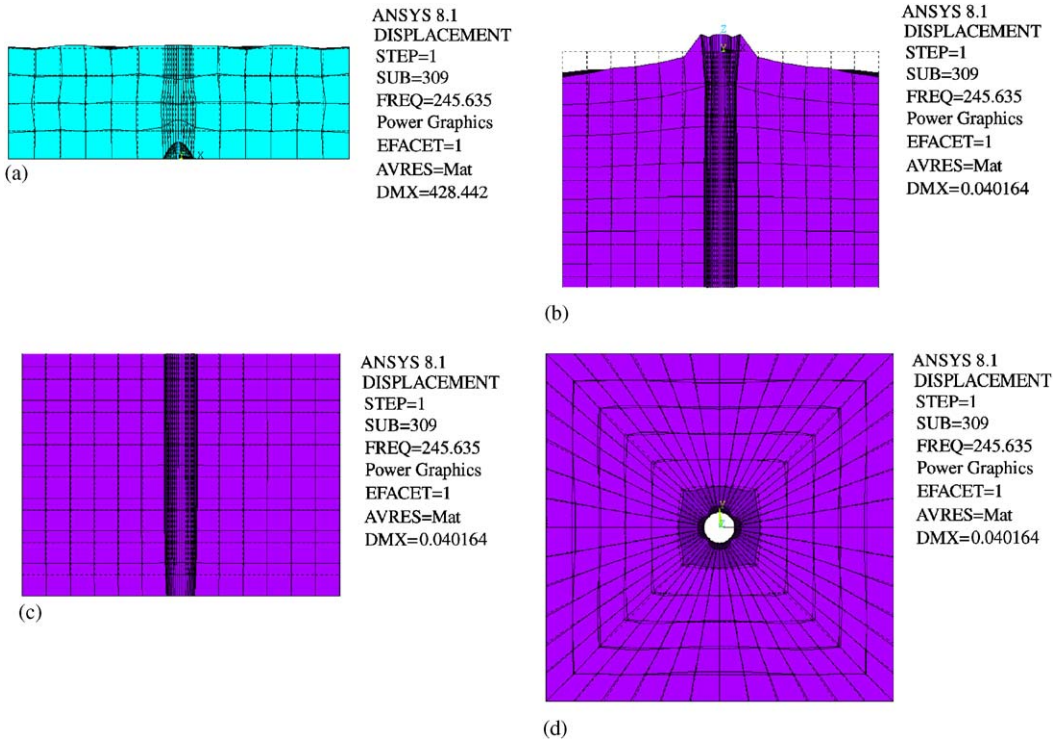

Fig. 19. Modal shape at 245.6 Hz in case 3: (a) modal shape of 1st layer; (b) upper part of 2nd layer; (c) lower part of 2nd layer; (d) top view of 2nd layer.

In case 2, the first structural mode of the layers is very close or matched to the deformed shapes of first two layers. The first modal shapes of two layers are shown in Fig. 18a and b, respectively.

In case 3, the 309th modal shape of the layers is found to close to the deformed shape of the first two layers shown in Fig. 17. The 309th modal shapes of two layers are shown in Fig. 19. Top view of the vibration mode of layer two as in Fig. 19d indicates that the number of circumferential waves is 4 for the cylindrical hole.

It is seen that different vibration modes of the layered structure are activated in case 2 and case 3 from Figs. 18 and 19. It means that the simulation-based analysis method of acoustic absorbent lining proposed in the paper can modify the material and structural properties of the absorbent lining to make it work in different vibration modes which leads to the desirable acoustic performance finally.

6. Conclusions

A simulation-based analysis method that combines acoustic FEM and acoustic duct method with a multi-variable, optimization technique is proposed for the design synthesis of acoustic absorbent lining. In the proposed method, a cell is extracted in isolation which may contain single

hole or a set of holes from whole periodic acoustic absorbent lining. Two acoustic ducts located above and below the cell are subsequently attached to the cell, respectively. The reflection and transmission characteristics of the acoustic absorbent lining are predicted using the acoustic duct theory. A zero-order optimization method is then applied to optimize the design parameters of the absorbent lining to achieve the desirable acoustics performance at the particular frequency of interest. Good agreement is found between the results from the proposed method and the analytical solutions for a homogeneous absorbent lining.

In the case studies conducted, two resonance mechanisms are observed for the acoustic absorbent lining with holes. When the absorbent lining works in the first resonance mechanism, the flexural motion of the first layer dominates the deformation of the absorbent lining as in case 2. The second layer which contains holes deforms mainly in thickness direction. When the absorbent lining works in the second resonance mechanism, the radial motion of the absorbent lining layer plays an important role in the deformation of the absorbent lining, while the first layer deforms not only in thickness direction but also in radial near the region above the hole in the second layer below. It is found that the radial deformation of the second layer around the hole has 4 numbers of circumferential waves. In case 3, the optimization of the geometrical and material properties of the acoustic absorbent lining brings the modal frequency of the layered structure much closer to the target frequency so that the anechoic effects of the optimized absorbent lining are better than the optimized absorbent lining in case 2.

Which resonance mechanism dominates the deformation of the absorbent lining depends on not only the comparative relations among the stiffness of three layers but also the geometrical parameters of the absorbent lining, such as hole size and layer thickness, etc. This observation differs that in Ref. [15].

The analysis on energy dissipation in the first two layers of the absorbent lining reveals that most of the vibration energy is dissipated by the first layer in both cases. However, the second layer of the absorbent lining in case 3 can dissipate much more vibration energy than the layer in case 2.

References

[1] H. Oberst, Resonant sound absorbers, in: E.G. Richardson (Ed.), *Technical Aspects of Sound*, Elsevier, Amsterdam, vol. 2, 1957.

[2] E. Meyer, K. Brendel, K. Tamm, Pulsation oscillation of cavities in rubber, *Journal of the Acoustic Society of America* 30 (1958) 1116–1125.

[3] G. Gaunaurd, One-dimensional model for acoustic absorption in a viscoelastic medium containing short cylindrical cavities, *Journal of the Acoustic Society of America* 62 (1977) 298–307.

[4] T.C. Ma, R.A. Scott, W.H. Yang, Harmonic wave propagation in an infinite viscoelastic medium with a periodic array of cylindrical elastic fibres, *Journal of Sound and Vibration* 69 (1980) 257–264.

[5] T.C. Ma, R.A. Scott, W.H. Yang, Harmonic wave propagation in an infinite elastic medium with a periodic array of cylindrical elastic fibres, *Journal of Sound and Vibration* 69 (1980) 473–482.

[6] A.C. Hennion, R. Bossut, J.N. Decarpigny, C. Audoly, Analysis of the scattering of a plane acoustic wave by a periodic elastic structure using the finite element method: application to compliant tube gratings, *Journal of the Acoustic Society of America* 87 (1990) 1861–1870.

[7] A.C. Hennion, J.N. Decarpigny, Analysis of the scattering of a plane acoustic wave by a doubly periodic elastic structure using the finite element method: application to compliant tube gratings, *Journal of the Acoustic Society of America* 90 (1991) 3356–3367.

[8] J.D. Achenbach, C.Y. Lu, M. Kitahara, 3-D reflection and transmission of sound by an array of rods, *Journal of Sound and Vibration* 125 (1988) 463–476.
[9] V. Easwaran, M.L. Munjal, Analysis of reflection characteristics of a normal incidence plane wave on resonant sound absorbers: a finite element approach, *Journal of the Acoustic Society of America* 93 (3) (1993) 1308–1318.
[10] C. Audoly, Global characterization of acoustic panels at normal incidence for underwater applications, *Acustica* 76 (1992) 129–136.
[11] G.R. Liu, C. Cai, K.Y. Lam, Sound reflection and transmission of compliant plate-like structures by a plane sound wave excitation, *Journal of Sound and Vibration* 230 (4) (2000) 809–824.
[12] C. Cai, G.R. Liu, K.Y. Lam, An exact method for analysing sound reflection and transmission by anisotropic laminates submerged in fluids, *Applied Acoustics* 61 (2000) 95–109.
[13] K. Peter, (Ed.), Theory Release 5.7, ANSYS Inc, 2001, pp. 20-10–20-14.
[14] R. Lane, Absorption mechanisms for waterborne sound in Alberich anechoic layers, *Ultrasonics* 19 (1981) 28–30.
[15] G. Gaunaurd, Comments on Absorption mechanisms for waterborne sound in Alberich anechoic layers, *Ultrasonics* 19 (1981) 90–91.